Nanopatterning and tuning of optical taper antenna apex for tip-enhanced Raman scattering performance

S. S. Kharintsev[1,a)], A. M. Rogov[1] and S. G. Kazarian[2]

[1] *Department of Optics and Nanophotonics, Institute of Physics, Kazan Federal University, Kremlevskaya, 16, Kazan, 420008, Russia*

[2] *Department of Chemical Engineering, Imperial College London, SW7 2AZ, United Kingdom*

This paper focuses on finding optimal electrochemical conditions from linear sweep voltammetry analysis for preparing highly reproducible tip-enhanced Raman scattering (TERS) conical gold tips with dc-pulsed voltage etching. Special attention is given to the reproducibility of tip apex shapes with different etchant mixtures. We show that the fractional Brownian motion model enables a mathematical description of the decaying current kinetics during the whole etching process up to the cutoff event. Further progress in preparation of highly reproducible smooth and sharp tip apexes is related to the effect of an additive, such as isopropanol, to aqueous acids. A FDTD-based near-field analysis provides evidence that TERS performance depends critically on tip orientation relative to a highly focused laser beam. A TERS based criterion for recognizing gold tips able to couple/decouple optical near- and far-fields is proposed.

a) Author to whom correspondence should be addressed. Electronic mail: skharint@gmail.com

I. INTRODUCTION

Fabrication and characterization of plasmonic optical nanoantennas, often referred to as a TERS active tips, are very important in single molecule spectroscopy and near-field imaging.[1-7] The commonly used tip fabrication technique - dc, dc-pulsed, ac voltage electrochemical etching, is a complex process governed by a large number of parameters which require optimization. Considerable advances achievable by different research groups[8-13] in optical nanoantennas design are mostly related to their mesoscopic zone rather than a tip apex being shaped in the final phase. It is evident that creation of tip apexes acting as hot spots for effectively coupling/decoupling optical near- and far-fields is worthy of special attention. They are at the heart of TERS techniques in parallel with the quality of laser beam modes. One should distinguish the reproducibility of an antenna's mesoscopic structure from that of the tip apex. The etching current cutoff event provides the basis for reliably fabricating smooth and sharp conical gold tips suitable for TERS performance and implementation. In connection with the unpredictable behavior of the current kinetics at the drop-off moment a lower reproducibility of tip apexes is obviously expected. Even though control of the tip apex production parameters would be good for TERS purposes its capacity to be a perfect far-to-near field coupler may still fail because of improper operation.[14] Such parameters as tip-sample distance, tip orientation relative to the laser spot and incident light polarization should be thoroughly aligned.

In this paper we report on optimal electrochemical conditions based on a linear sweep voltammetry (LSV) analysis for preparation of TERS active gold tips with dc-pulsed voltage etching in different background electrolytes. In order to gain a clearer understanding of tip apex shaping an etchant of hydrochloride acid and doubly-distilled water at various volume ratios is used. The effect of additives, such as, isopropanol to the etchant mixture was also investigated.

To quantitatively characterize the current kinetics we introduce the fractional Brownian motion model which is the best fit to describe decaying current curves. The current kinetics are governed by the scaling equation and, thus, they are self-similar. This model provides the benefit of understanding of the shaping of the tip apex during the whole etching process up to the drop-off event. Finally, of fundamental importance is to verify that well-shaped tips act as hot spots and are suitable for performing TERS measurements. We show that the capacity for far-to-near field coupling is dramatically dependent upon tip orientation with respect to the focal plane of incident light. TERS active gold tips are tested with near-field Raman scattering of oxide graphene flakes rather than Rayleigh backscattering detected with 2D confocal microcopy. A noticeable difference in optical and Raman maps is followed by the four-fold field enhancement for Raman scattering.

II. RESULTS AND DISCUSSION

A. DC-pulsed electrochemical etching

Electrochemical dc-pulsed etching of a gold wire is performed with a home-built voltage controller and a three electrode electrochemical cell with a internal bottom-free glass beaker, as shown in Fig. 1(a). The schematic is not drawn to scale. In our etching experiments we used a Ag/AgCl (~0.22V) reference electrode. A commercial potentiostat μ-Autolab III (Autolab, The Netherlands) is utilized for performing LSV analysis. Figure 1(b) shows, for comparison, LSV curves for the two and three electrode cells for a HCl/Ethanol (50:50 vol.%) etchant that has proven to be a striking finding of Ren's group.[8,13] A 100 μm gold wire (purity: 99.99%, GoodFellow, UK) as a working anodic electrode is symmetrically positioned into the beaker with a piezoelectric translation stage NTS10 (DTI, USA) by a value of 1.5 mm in depth with an

accuracy of 125 nm. A gold counter ring 2 mm thick electrode with a diameter of 15 mm is entirely submerged by a depth of 10 mm into a solution of fuming hydrochloric acid (HCl, 37%) and doubly distilled water. The volume of an etchant is 160 ml and is maintained at a room temperature of 20^{o}C.

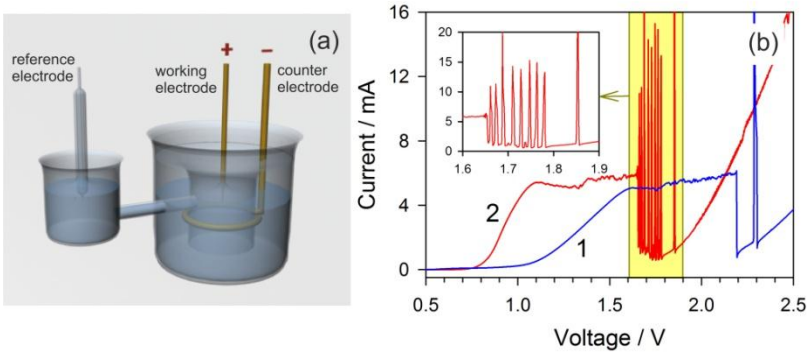

FIG. 1. Schematic view of a three electrode electrochemical cell (a), linear sweep voltammetry of a gold wire in a solution of HCl and ethanol in a proportion of 1:1 (b) for two electrode scheme (blue curve 1) and three electrode cell (red curve 2). Current oscillations above an electrode potential of ~1.68 V for gold are shown in the inset.

A square voltage wave facilitates mechanical mixing of the etchant near the meniscus. Voltage values, pulse duration and duty cycle are important parameters for dc-pulsed electrochemical etching gold wires. Up and down voltage values of U_{down} and U_{up} can be determined from an analysis of linear sweep voltammetry curves at a rate of 0.1 V/s as shown in Fig. 2(a) for various HCl/water volume ratios. The etching current increases as the HCl concentration is increased. An abrupt drop in current above a voltage of 1.9 V is caused by the formation of chloroaurate complexes $\mathrm{AuCl}_{4-x}[\mathrm{OH}]_x^-$ followed by oxidation reactions: 1) $\mathrm{Au} \leftrightarrow \mathrm{Au}^{3+} + 3\mathrm{e}^-$ and 2) $\mathrm{Au} \leftrightarrow \mathrm{Au}^{+} + \mathrm{e}^-$ at electrode potentials of ~1.5 V and ~1.68 V,

respectively.[10] This passivation layer slows down the electrochemical etching because of the depletion of oxidizing agents, Cl^-, near the gold surface.[8,13]

Further increasing the voltage causes a smooth rise in etching current which undergoes well-defined oscillations.[8,13,15] These features of the LSV curves are explained by the production and release of Cl_2 and H_2 bubbles on the anode and cathode and thus cell resistance fluctuates strongly. The bubbling effect negatively affects the reproducibility of well-shaped tip apexes

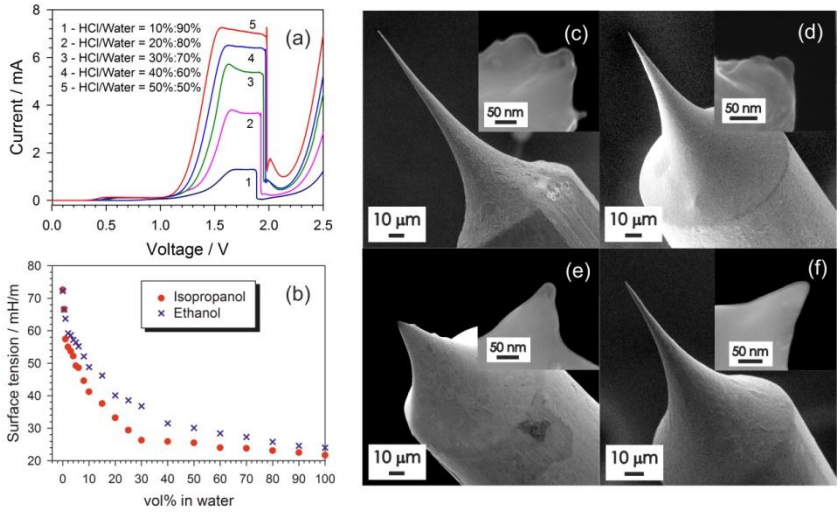

FIG. 2. (a) - Linear sweep voltammetry of a 100 µm gold wire in a HCl/Water mixture at different ratios. (b) - Surface tension of isopropanol and ethanol diluted with water vs. volume ratios. SEM images of gold tips and their apexes electrochemically etched in: (c) - HCl/Water = 30:70 vol.%, (d) - HCl/Water (40:60 vol.%), (e) - HCl/Water (50:50 vol.%) and (f) - HCl/Water/Isopropanol (50:45:5 vol.%).

making them blunt and rough. LSV curve 2 in Fig. 1(b) demonstrates current oscillations above a voltage of ~1.68 V in the vicinity of the working electrode for a HCl/Ethanol (50:50 vol.%), as reported in Refs[8,13]. It provides evidence that oxidation with $Au \leftrightarrow Au^+ + e^-$ represents a major corrosion mechanism. One should notice that current oscillations increases with HCl concentration for different dilutes. In the case of the two electrode cell a voltage plateau up-shifts by a value of ~0.5 V. The latter depends upon the working/counter electrodes, the chemical

nature of the etchant and its volume. This means that an optimal voltage range is fair only for the given parameters. In the two electrode scheme we observe a fewer current oscillations due to such contributions as electrode potential, ohmic drop and electrode polarization into the emf of the cell. Based on an analysis of LSV curves (Fig. 2(a)) the up voltage, U_{up}, is chosen below a value at which the current drops, that is, ~1.9 V. Importantly, therefore, current oscillations are avoided throughout the etching. The meniscus vicinity enriches with chloride anions at down voltage, U_{down}, due to diffusion of corrosion products. However, too low values of the voltage result in vanishing currents and the current cutoff event comes untimely. As a consequence, unfinished tips to be utilized in near-field experiments come into the reality. Therefore, the down voltage value is commonly favorable within the range of 1-1.6 V. In our study the value of 1.5 V was used.

SEM images of dc-pulsed electrochemically etched gold tips with a duty cycle of 0.5 and a pulse duration of 250 ms are shown in Fig. 2 (c), (d) and (e) for various volume ratios. Their radii of curvature lie in the range of 15-25 nm as follows from Fig. 2(c)-(f). It is easily seen that at low concentrations of HCl the tip apex surface looks rough and, as a consequence, it yields a low reproducibility of well-defined apex shapes. With increasing HCl concentration the aspect ratio of the tip shaft reduces reliably and the tip apexes produced becomes smoother and sharper. The extended and concave-shaped cones are stipulated by a high value of surface tension for water (71.8 mH/m at 25^{o}C) as shown in Fig. 2(b). Higher HCl concentrations (>60 vol.%) result in smooth and blunt tip apexes due to higher cutoff current values of >5 mA and shorter etching time values of ~40-60 s. This infers that the best results from the reproducibility viewpoint might be reachable for the HCl/Water etchant in a proportion of 40:60 vol.%.

At the end of the etching process fluctuations in gold wire resistance increase and enhanced mixing at the meniscus is desirable. This could be achieved by reducing the surface tension of the etchant. For this purpose ethanol (23.6 mH/m at 25^{o}C) or isopropanol (21.7 mH/m at 25^{o}C) are best suited as a diluent (Fig. 1(b)). The latter is preferable to uniformly regulate the surface tension in a wide range of 25-70 mH/m. Figure 2(f) shows a SEM image of a tip shaft and apex etched with a solution of HCl/Water/Isopropanol (50:45:5 vol.%). It has been found experimentally that the admixture improves the reproducibility of the tip apex up to ~70% to be smooth and as sharp as of ~10-30 nm (Fig. 1(f)). A number of tips prepared with each etchant was equal to 10. It is important to stress that, unlike the approach proposed in Ref.[10], no add-on procedures for selecting successful tips are used.

B. Self-similar behavior of etching current

In general the etching current through the gold wire immersed in the etchant as a function of time $I(t)$ satisfies the following scaling equation[16]

$$I(\xi t) = \gamma I(t), \tag{1}$$

where ξ is a scaling parameter, γ is a factor. A solution of Eq.(1) reads as

$$I(t) = a t^{-\mu} = a t^{\alpha + i\beta}, \tag{2}$$

where μ is a complex exponent, α and β are real exponents, a is a factor. To further approximate decaying current curves while a square wave voltage we will utilize the relationship[15]

$$I(t) = \mathrm{Re}\left[I_0 + a t^{-\mu}\right] = I_0 + a t^{\alpha} \cos[\beta \ln(t)], \tag{3}$$

since an initial etching current I_0 exists at $t = 0$. Eq. (3) corresponds to the Fractional Brownian motion model, in which current kinetics are considered to be self-similar. This means that the

current at a given time is dependent on previous values taken at times iteratively calculated from the temporal Cantor set.[16] The presence of inherent log-periodic oscillations ($I(t) \sim \cos[\beta \ln(t)]$) are stipulated by anomalous diffusion of chloride anions. The physical interpretation of α and β remains challenging. We suppose that the former might be referred to as a transport parameter for chloride anions through a passivation layer, whereas the latter characterizes losses of Cl^- to be ready to attack the wire surface.[15]

Figure 3(a) shows least-squares fitting of decaying current curves with Eq. (3) when a square wave voltage is applied. One should notice that the physical model has proved to be adequate to fit experimental data best of all during the whole etching. Behaviors of α and β parameters for various etchants are given in Fig. 3(b) and (c). As it follows from the figure the current kinetics for a HCl/water etchant is determined by $I(t) \cong I_0 + a t^{-1/2}$, in other words the transport of chloride ions to the wire surface is governed by conventional Brownian motion. This approximation is fair at the end of etching ($\beta \approx 0$), whereas this parameter is strongly scattered at early times. Importantly, the Pearson correlation of experimental data and the fitting function is better than 0.999 except when close to the drop-off event. This discrepancy is related to the small surface area at the meniscus where etching more greatly corrosive and the current strongly fluctuates because of the bubbling effect. Formally, the whole etching might be divided into two regions: one corresponds to a mesoscopic zone, the other to a tip apex zone (Fig. 3(d)). This drawback might be eliminated by reducing the surface tension of an enchant and, thus, it would lead to the negligible bubbling effect. Isopropanol was added into the etchant of HCl/water in an attempt to stabilize etching at the final stage. Figures 3(b), (c) and (d) show a good fit of Eq.3 to experimental data, the Pearson correlation is better than 0.999 throughout the etching. In that case the etching time is twice shorter, it typically takes approximately ~40-50 s. The α

parameter approaches $-1/2$ at the current cutoff event, as happens for the HCl/water etchant. Of importance is the behavior of the β parameter, it monotonically drops down to $1/2$ meaning that there is uninterrupted access of Cl^- towards the meniscus. On the other hand, the current kinetics are satisfactorily fitted with a three parametric analytical model $I(t) = I_0 + a t^{\alpha} \cos\left[\ln\left(\sqrt{t}\right)\right]$ for a HCl/water/isopropanol (50:45:5 vol%) etchant. Finally, Eq.(3) clearly shows the fractal behavior of the current kinetics over the whole etching including times at which the tip apex is eventually being shaped.

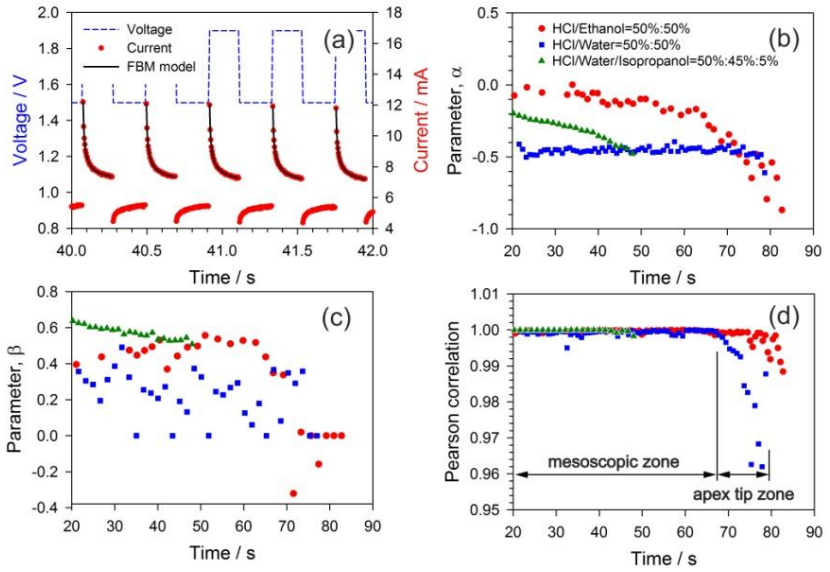

FIG. 3. (a) - Etching current kinetics under a square wave voltage for HCl/Water (50:50 vol.%). Fitting parameters α (b) and β (c) from Eq. 2 for various etchants. (d) - Pearson correlation vs etching time for various etchants.

C. Tip inclination effect

The next step was to test electrochemically etched gold tips for TERS activity. This means that we want to find those of them that enhance a total backscattered intensity by a magnitude of more than 2. This factor is due to dual scattering in a tip-sample system. Under TERS-active tips

we understand antennas capable to enhance and localize a laser light due to the plasmonic effect. For this purpose we use a hybrid scanning probe microscope equipped with an optical

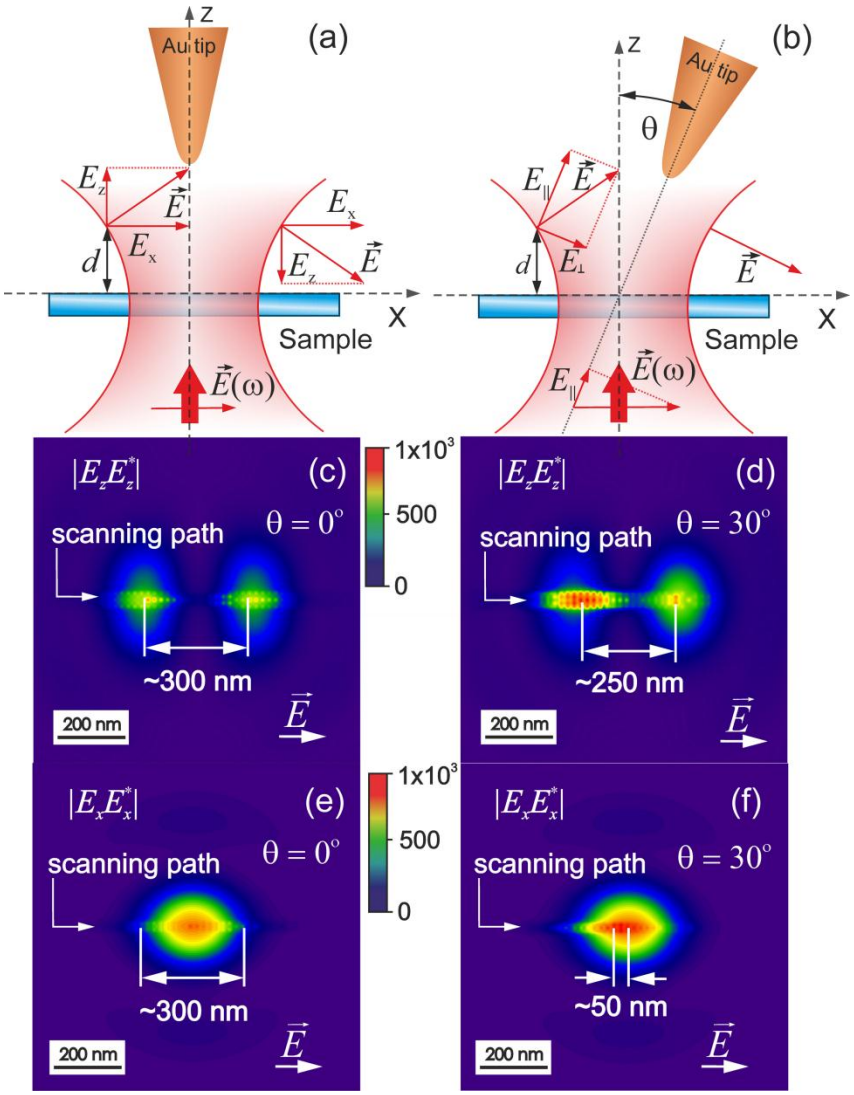

FIG. 4. Tip orientation relatively to the optical z-axis: (a) - 0°, (b) - at θ angle. Calculated two-dimensional map of $\left|E_z^2\right|$ and $\left|E_x^2\right|$ enhanced with a gold tip oriented relatively the z-axis at different angles: $\theta = 0^\circ$ (c),(e) and $\theta = 30^\circ$ (d), (f).

spectrometer NTEGRA SPECTRA™ (NT-MDT, Russia). Prepared tips of 2 mm in length are thoroughly glued to a tuning fork that oscillates at a resonance frequency of ~192 kHz perpendicularly to the sample plane. Importantly, the tuning fork is mounted at a holder under an

angle of 10° to the sample plane. We rejected all tip-equipped quartz tuning forks with a Q-factor of less than 500. Further, the tip is carefully approached to the surface and kept at a constant height of ~3-10 nm by shear force control. In the inverted optical scheme a highly focused laser beam is used for probing hot spots with longitudinal modes of the electric field as schematically shown in Fig 4(a). This is easily reached with a x100 oil immersion objective with a high numerical aperture of 1.4. Our motivation is to couple a gold tip and the laser spot for gaining the TERS effect. As mentioned above the main obstacles in the TERS performance and implementation are tip geometry, tip orientation and the quality of a laser beam.[17,18] Traditionally, the alignment of the tip relative to the focal spot in the inverted configuration is implemented with backscattering reflection microscopy technique when the tip is raster scanned over a sample. An optical response is registered with a photo multiplier tube (Hamamatsu, Japan). The reflection pattern is followed by tip inclination with respect to the z-optical axis. To provide deeper understanding of this effect we have performed FDTD numerical calculations of $\left|E_z^2\right|$ and $\left|E_x^2\right|$ when the tip is oriented in parallel (Fig. 4(c),(e)) and under an angle of 30° (Fig. 4(d),(f)) to the z-axis and is raster scanned at a step of 25 nm along a straight line coinciding with the polarization direction of linearly polarized laser light (TEM_{00}) with a wavelength of 632.8 nm. The latter is tightly focused with the help of a high numerical aperture lens. In our simulation we used the following tip parameters: curvature radius of 20 nm, cone angle of 45° and tip-sample distance of 6 nm. As soon as the tip passes over one of the longitudinal lobes the net squared field enhancement factor reached ~ 800.[19] The distance between two maxima located at the rims of the diffraction-limited spot is estimated to be $\sim \lambda/2 \approx 300\,\text{nm}$. Tip inclination results in a stronger field enhancement in one of the lobes in which the electric field direction is very close to the tip axis, whereas in other direction the field strength weakens since

the tip meets s-polarized light (Fig. 4(b)). In other words, a direction of the electric field is perpendicular to the tip axis. Thus, we observe an asymmetry in the field strength between two lobes which move towards each other. A tip-angle-dependent lobe position shift by a magnitude of ~50 nm takes place. Figure 4(f) shows the same shift for the $\left|E_x^2\right|$ maximum towards the left rim of the laser spot. A supplementary effect is observed due to localized surface plasmons excitation with the transverse component of the electric field. A contribution of its projection $E_{||}$ on the tip axis to the field enhancement, being maximal at the core of the laser beam, vanishes towards the right rim of the laser beam. It means that the distance between two lobes on a total integrated intensity reflection image may be twice reduced down to $\sim\lambda/4\approx150\,\mathrm{nm}$ or less depending on tip inclination. A hot spot region spreads and the electric field increases in one of the longitudinal lobes and, thus, the observed asymmetry[17,18] in the lobes for an "ideally" tuned laser beam is followed by the tip inclination effect. Transverse and longitudinal near-field contributions to the total backscattering intensity are comparable due to a plasmonic nanoantenna.

D. TERS activity criterion

Figure 5 shows experimental evidence of tip inclination for gold conical nanoantennas prepared with different etchants. TEM images of the tip apexes under study are given in Fig. 5(a), (b) and (c). As seen from the figure all tips are covered with an amorphous carbon contamination layer. However, for tips prepared with HCl/Water etchant a layer structure in the vicinity of their apexes is noticeably non-uniform. We suppose that chloroaurate complexes' remains after etching contribute to the layer. So far, the influence of the contamination layer on TERS activity of gold tips has been debated[20].

Prepared gold tips have been visualized with 2D confocal optical microscopy with a pinhole of 25 nm and an exposure time of 750 ms per a pixel (see Fig. 5 (d), (e) and (f)). We clearly observe ambiguity in selecting a proper hot spot. This obstacle appears in both shear force configurations: 1) a tip oscillates vertically (tapping mode operation) and 2) it "sweeps" horizontally in respect to the sample plane. Unfortunately, we cannot govern tip orientation in our experiment. It especially concerns the tapping mode. A little tip tilt of $<5^{o}$ appears when gluing the tip on a tuning fork and there is the tuning fork inclination of $\sim 10^{o}$-20^{o} relative to the sample plane because of a shear force head orientation. A less intensive lobe in Fig. 5(d) is followed by the transverse electric field and being located at the z-axis. In this situation we bring a tip into a more bright spot. In other cases this is complicated by the fact that the lobes cannot be resolved at all as shown in Fig. 5(e).

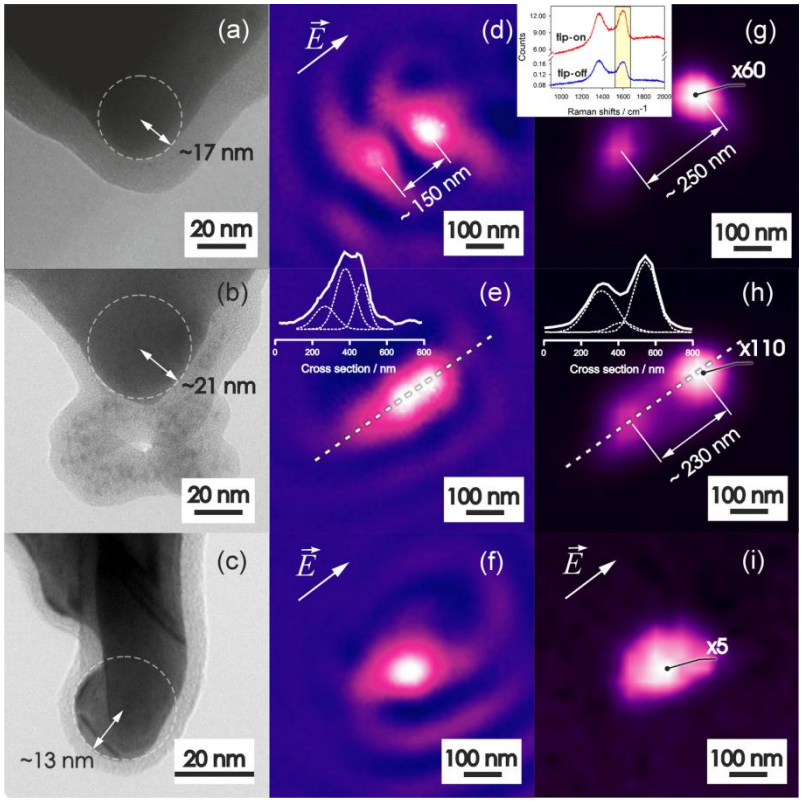

FIG. 5. TEM images of tip apexes electrochemically etched with HCl/Water/Isopropanol (50:45:5 vol.%) (a), HCl/Water (50:50 vol.%) (b) and HCl/Ethanol (50:50 vol.%) (c). Confocal optical images of tip

apexes electrochemically etched with HCl/Water/Isopropanol (50:45:5 vol.%) (d), HCl/Water (50:50 vol.%) (e) and HCl/Ethanol (50:50 vol.%) (f), near-field Raman images of tip apexes electrochemically etched with HCl/Water/Isopropanol (50:45:5 vol.%) (g), HCl/Water (50:50 vol.%) (h) and HCl/Ethanol (50:50 vol.%) (i) at 1590 cm^{-1} as indicated in the inset in Fig. 5(g).

Certainly one can decompose a cross section into individual Gaussian peaks with the least squares method and observe two longitudinal lobes and one transverse lobe (see inset in Fig. 5(e)). Anyway the tip position accuracy will be low for effectively far-to-near field coupling. To avoid the uncertainty we propose the following TERS-based criterion for detecting hot spots. It is important to emphasize that the criterion allows one to only find well-defined tips to be TERS active rather than to optimize the TERS active tips for better reproducibility.

A slide cover glass is covered with a homogeneous thin film for which a Raman spectrum is well studied. As a suitable material we have used graphene oxide flakes prepared by spin-coating 30 times a diluted 2 wt% single layer graphene oxide water dispersion (US Research Nanomaterials, USA) at 1500 rpm for 2 min. The laser power at the sample was of order of ~50 μW. All 128x128 pixel maps were captured with an electron multiplying charge coupled device detector (Andor, UK) cooled down to -80 ºC. The exposure time of 0.1 s per a pixel was used.

Figures 5 (g), (h) and (i) show the near-field Raman maps at ~1590 cm^{-1} (as marked in the inset) while a gold tip is raster scanned over the focal spot. Two lobes spaced at a distance of approximately 250 nm are distinctly observed in Fig. 5 (g) and (h). An asymmetry in the total integrated intensity of hot spots is evidence of tip inclination. Obviously, in a perfect arrangement when a tip is aligned to be perpendicular to the sample plane the hot spots positions coming from confocal optical microscopy and near-field Raman microscopy should necessarily coincide. A considerable difference in the optical contrasts might be caused by the four-fold field enhancement ($g^4 = \left|\vec{E}_{sc}(\omega_{inc})/\vec{E}_{inc}(\omega_{inc})\right|^4$, $\vec{E}_{sc}(\omega)$ is an electric field of a scattered wave,

$\vec{E}_{inc}(\omega)$ is an electric field of an incident wave, ω_{inc} is a frequency of an incident wave, that is very close to that of a scattered wave ω_{sc}, that is, $\omega_{inc} \approx \omega_{sc}$) for Raman scattering.[21,22] Despite the fact that the underlying four-fold field-enhancement mechanism is still debated, we conjecture that the clearly observable longitudinal lobes in the Raman pattern, that are located at the rims of the diffraction-limited laser spot, are stipulated by the enhancement of both incident and scattered light. As follows from the inset of Fig. 5(h), a cross section through the lobes decomposed into three individual components with the least squares method reveals high intensity longitudinal lobes at the rims of a highly focused laser beam and a low intensity transverse mode at the center. This is possible due to the enhancement of scattered light from a molecule with polarizability towards the z-axis. A higher field enhancement factor F, estimated as[23] $F = \left(I_{near}/I_{far}\right)\left(\lambda^2/L^2\right)$ (where I_{near} and I_{far} is a near- and far-field intensity, λ is an incident light wavelength, $L = \sqrt{2rh}$ is a near-field extent beneath the tip apex, r being a curvature radius of the tip apex, h is a tip-sample spacing) and equal to ~60 (Fig. 5(g)) and ~110 (Fig. 5(h)), in one of the lobes is followed by a tip tilt in such a way that it meets p-polarized light optimally. Our numerous experiments (10 tips with each etchant under the same conditions) have shown the efficiency of TERS active gold tips to be equal to approximately 50%. This estimate tells us that only 5 gold tips were capable of the field enhancement beneath the tip apexes. A backscattered reflection and Raman pattern, shown in Fig. 5(f) and Fig. 5(i), correspond to each other, we observe only one lobe positioned at the optical axis. The enhancement factor of ~5 is related to the electrostatic lightning-rod effect caused by purely geometric singularity of the tip apex. A such tip is considered to be non-TERS active one. Thus, even if an electrochemically etched tip turns out to be well-defined in a geometrical sense, its

capacity to enhance incident and/or scattered light should be necessarily verified with the TERS activity criterion prior to near-filed measurements implementation.

III. CONCLUSION

In conclusion, we would like to highlight that one should steadily optimize an electrode potential or voltage in terms of the linear sweep voltammetry for an etchant of interest. In order to achieve a high yield of well-shaped tip apexes a stationary behavior of decaying current curves at the cutoff event must be maintained. Current kinetics are governed by a scaling equation over the whole etching time. This can be achieved by reducing the surface tension of a mixture of HCl/Water with, in our study, isopropanol. This admixture improves the reproducibility of tip apexes up to >70% making them smooth and sharp (10-30 nm radii of curvature at the apex. However, a lower yield of TERS active tips is caused by tip orientation relative to a laser spot and a laser beam quality. We have suggested a TERS based criterion for effective coupling of near and far optical fields. A near-field Raman map of an apex tip at ~1590 cm^{-1} on graphene oxide flakes allows one to securely find a hot spot compared to that from a 2D confocal optical image. In particular, a difference in optical contrasts distinctly proves the four-fold field enhancement for near-field Raman scattering. Finally, the reproducibility of well-defined tips and their apexes is estimated to be >95% and ~70%, respectively, and only half of them were able to enhance and squeeze laser light due to localized surface plasmon excitation.

ACKNOWLEDGEMENTS

The authors thank Prof. Alexander Fishman (Kazan Federal University), Dr. Alexei Noskov (Kazan Federal University) and Dr. Jennifer Dougan (Imperial College London) for

support and assistance in preparing of the paper. This study was financially supported by the Russian Foundation for Basic Research (No. 13-02-00758 A).

REFERENCES

[1] P. Bharadwaj, B. Deutsch, L. Novotny, Advances in Optics and Photonics, **1**, 438 (2009).

[2] M. Sonntag, J. Klingsporn, L. Garibay, J. Roberts, J. Dieringer, T. Seideman, K. Scheidt, L. Jensen, G. Schatz, R. Van Duyne, J. Phys. Chem. C, **116**, 478 (2012).

[3] Y. You, N. Purnawirman, H. Hu, J. Kasim, H. Yang, C. Du, T. Yu, Z. Shen, J. Raman Spectrosc., **41**, 1156 (2010).

[4] H. Hayazawa, T. Yano, S. Kawata, J. Raman Spectrosc., **43**, 1177 (2012).

[5] R.M. Stockle, Y.D. Suh, V. Deckert, R. Zenobi, Chem. Phys. Lett. **318**, 131 (2000).

[6] N. Hayazawa, Y. Inouye, Z. Sekkat, S. Kawata, Chem. Phys. Lett. **335**, 369 (2001).

[7] B. Pettinger, B. Ren, G. Picardi, R. Schuster, G. Ertl, Phys. Rev. Lett. **92**, 096101-1 (2004).

[8] B. Ren, G. Picardi, B. Pettinger, Rev. Sci. Instrum. **75**, 837 (2004).

[9] L. Eligal, F. Culfaz, V. McCaughan, N. Cade, D. Richards, Rev. Sci. Instrum., **80**, 033701 (2009).

[10] S.S. Kharintsev, A.I. Noskov, G.G. Hoffmann, J. Loos, Nanotechnology, **22**, 025202 (2011).

[11] M.G. Boyle, L. Feng, P. Dawson, Ultramicroscopy, **108**, 558 (2008).

[12] G. Xu, Z. Liu, K. Xu, Y. Zhang, H. Zhong, Y. Fan, Z. Huang, Rev. Sci. Instrum., **83**, 103708 (2012).

[13] X. Wang, Z. Liu, M. Zhuang, H. Zhang, X. Wang, Z. Xie, D. Wu, B. Ren, Z. Tian, Appl. Phys. Lett., **91**, 101105 (2007).

[14] S. Berweger, M.B. Raschke, Anal Bioanal Chem., **396**,115 (2010).

[15] S.S. Kharintsev, G.G. Hoffmann, A.I. Fishman, M.Kh. Salakhov, J. Phys. D: Appl. Phys., **46**, 145501 (2013).

[16] R.R. Nigmatullin, A. Le Mehaute, J. Non-Crystalline Solids, **351**, 2888 (2005).

[17] R.V. Maximiano, R. Beams, L. Novotny, A. Jorio, L.G. Cancëado, Phys. Rev. B, **85**, 235434 (2012).

[18] A. Bouhelier, M.R. Beversluis, L. Novotny, Appl. Phys. Lett., **82**, 4596 (2003).

[19] D. Roy, J. Wang, C.J. Williams, J. Appl. Phys., **105**, 013530 (2009).

[20] K.F. Domke, D. Zhang, and B. Pettinger, J. Phys. Chem. C **111**, 8611 (2007).

[21] B. Sick, B. Hecht, U.P. Wild, L. Novotny, J. Microscopy, **202**, 365 (2001).

[22] R. Esteban, M. Laroche, J.-J. Greffet, J. Appl. Phys., **105**, 033107 (2009).

[23] D. Roy, J. Wang and C. Williams, J. Appl. Phys., **105**, 013530 (2009).